Electric *g* tensor control and spin echo of a hole-spin qubit in a quantum dot molecule

Robert Roloff[1,3]**, Thomas Eissfeller**[2]**, Peter Vogl**[2] **and Walter Pötz**[1]

[1] Fachbereich Theoretische Physik, Institut für Physik, Karl-Franzens Universität Graz, Universitätsplatz 5, 8010 Graz, Austria
[2] Walter Schottky Institut, Technische Universität München, 85748 Garching, Germany
E-mail: robert.roloff@uni-graz.at

Abstract. The feasibility of high-fidelity single-qubit operations on a hole spin in a quantum dot molecule by electric *g* tensor control is demonstrated. Apart from a constant external magnetic field the proposed scheme allows for an exclusively electric control of the hole spin. Realistic electric gate bias profiles are identified for various qubit operations using process-tomography-based optimal control. They are shown to be remarkably robust against decoherence and dissipation arising from the interaction of the hole with host-lattice nuclear spins and phonons, with a fidelity loss of $\approx 1\%$ for gate operation times of ≈ 10 ns. Spin-echo experiments for the hole spin are modeled to explore dephasing mechanisms and the role of pulse-timing imperfections in the gate fidelity loss is discussed.

[3] Author to whom any correspondence should be addressed.

Contents

1. Introduction

We propose and study the feasibility of all-electric control of a qubit realization based on the hole spin in a quantum dot molecule (QDM). This system offers two main advantages over electron-spin-based realizations: the use of hole spins increases the dephasing time associated with the interaction with nuclear spins by about an order of magnitude and allows for an efficient g tensor control, thereby facilitating essentially all-electric control of the qubit.

Spin-based quantum bit realizations in semiconductor quantum dots (QDs) have gained wide interest in the quantum computing community due to their potential regarding scalability and their long relaxation times. Most work, both theoretical and experimental, has focused on electron spin qubits, which have spin relaxation times ranging from several milliseconds [1] to seconds [2]. However, it has turned out that this type of qubit is prone to decoherence processes due to the interaction with surrounding nuclear spins of the host lattice [3, 4]. The Fermi contact hyperfine interaction ultimately limits the inhomogeneous dephasing time to $T_{2,e}^* \approx 10$ ns [5]. Several techniques to circumvent this problem have been devised, e.g. nuclear state preparation [6]–[9], fabrication of silicon-based semiconductor heterostructures with zero nuclear magnetic moment [10] or employing hole spins instead of electron spins [11, 12]. The p-type symmetry of the hole Bloch function leads to cancellation of the Fermi contact hyperfine interaction. However, it has been shown that the dipole–dipole hyperfine interaction and the coupling of the hole orbital angular momentum to the nuclear spins cannot be neglected [13]–[15]. These lead to an inhomogeneous dephasing time $T_{2,h}^*$ one order of magnitude longer than that of electrons [14], which is in good agreement with recent experiments [16].

Basic spin qubit implementation schemes usually require local magnetic fields for individual spin manipulations [17]. Another technique, which has been proposed and tested recently, is to exploit the tunability of electron-spin and hole-spin g tensors by electric fields rather than employing control by local magnetic fields [18]–[21]. If an external magnetic
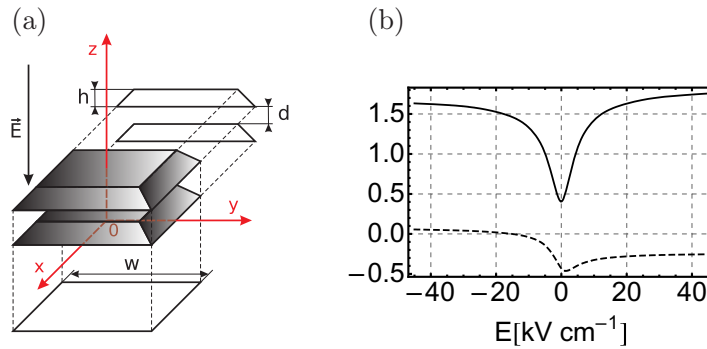
Figure 1. (a) Vertically stacked pyramidal QDs, dot spacing $d = 1.5$ nm, height $h = 2.5$ nm and width $w = 15$ nm. The coordinates x, y and z denote the [100], [010] and [001] directions, respectively. The origin of the coordinate system is indicated by 0. The external electric field points along the [001] direction, i.e. $\vec{E} = (0, 0, E)$. (b) Electric field dependence of the g tensor elements. The solid and the dashed line denote $g^{001}(E)$ and $g^{1\bar{1}0}(E)$, respectively. (Data are taken from [21].)

field $\vec{B}$ is present, the spin experiences an effective field $g(E) \cdot \vec{B}$ that can be changed locally by means of the electric field E. The dependence of the g tensor on E is particularly pronounced for hole spins in vertically stacked QDMs since the localization of the hole wavefunction is very sensitive to externally applied electric fields [21]. The goal of this paper is to show that in such a system, unitary single-qubit gates can be efficiently realized for simple pulse shapes of 10 ns duration.

In section 2, we describe the computational basis states of the qubit, the corresponding Hamiltonian and the mechanisms that lead to non-unitary dynamics. The equation of motion for the qubit, including decoherence and relaxation dynamics, is given. In section 3, we apply optimal control theory in order to find simple electric pulse shapes that execute the Hadamard gate, as well as a $\pi/2$ and a π pulse. We find that these transformations can be implemented with remarkably low fidelity losses of $\approx 1\%$. In addition, we show how spin-echo experiments can be performed on the hole spin to explore decoherence in the system. We also discuss quantitatively the effect of pulse-timing imperfections. We conclude with a summary of the present work. The model for the interaction of the nuclear spins with the hole is detailed in appendices A and B.

2. Theory

In this section, we present the qubit realization and give the effective Hamiltonian for a single hole in a QDM composed of vertically stacked self-assembled InAs/GaAs QDs separated by a small tunnel layer. The detailed geometry of the QDM, which we use for the present study, is shown in figure 1(a). Two pyramidal dots (height h, width w) are stacked on top of each other and separated by a barrier of distance d. The QDM is exposed to a static magnetic field, as well as a time-dependent electric field applied along the [001] growth direction. It is controlled by a gate bias and used to modulate the hole g factor by shaping the hole wavefunction [21]. The controlled growth of InAs/GaAs QDMs as well as the electric modulation of exciton g factors in such structures has been demonstrated experimentally in [19].

Next to the interaction of the hole with the externally applied control fields, all contained in the effective Hamiltonian H_0, there will be additional (unwanted) interactions with the solid-state environment. Therefore, we account for the interaction of the host-lattice nuclear spins with the hole, develop a phenomenological description of the hole–phonon interaction and give the resulting equation of motion on which our analysis is based.

The first task is to compute the effective interaction of the hole with a constant external magnetic field. The interaction is characterized by a g tensor, which depends on the externally applied electric field, as shown in figure 1(b) [21]. We have performed three-dimensional 8-band envelope function calculations, including external fields, strain and piezoelectric polarization, in order to determine the QDM heavy-hole and light-hole components of the ground $|\Psi_0\rangle$ and the first excited Zeeman state $|\Psi_1\rangle$. Details of this method have been published elsewhere [22, 23]. For a vertical external magnetic field, the energy eigenstates $|\Psi_0\rangle$ and $|\Psi_1\rangle$ of the full 8×8 Hamiltonian correspond predominantly to heavy-hole (hh) down ($j_z = +3/2$) and hh up ($j_z = -3/2$) states, respectively. The conduction and split-off (SO) band contributions are neglected, since they are $\lesssim 1\%$. However, light-hole (lh) contributions *cannot be neglected*. We write the hole wavefunctions as

$$\langle\vec{r}|\Psi_k\rangle \equiv \Psi_k(\vec{r}) = \sqrt{\Omega} \sum_{j,j_z} F^{(k;j,j_z)}(E,\vec{r})\psi^{(j,j_z)}(\vec{r}),$$

$$j \in \left\{\frac{3}{2},\frac{1}{2}\right\}, \quad j_z \in \left\{\pm\frac{3}{2},\pm\frac{1}{2}\right\}, \quad k \in \{0,1\}, \tag{1}$$

where $F^{(k;j,j_z)}(E,\vec{r})$ denotes the envelope function associated with the Γ-point basis function $\psi^{(j,j_z)}(\vec{r})$, which transforms like the eigenfunction $|j,j_z\rangle$ of the angular momentum operator J_z, and Ω is the volume of the unit cell of the crystal. For zero electric field $\vec{E}$ and for vertical magnetic field $\vec{B} = (0, 0, 10)$ mT, the hh and lh contributions, respectively, are given by

$$\int d\vec{r} \left\{|F^{(k;3/2,+3/2)}(E,\vec{r})|^2 + |F^{(k;3/2,-3/2)}(E,\vec{r})|^2\right\} \approx 0.909,$$

$$\int d\vec{r} \left\{|F^{(k;3/2,+1/2)}(E,\vec{r})|^2 + |F^{(k;3/2,-1/2)}(E,\vec{r})|^2\right\} \approx 0.075, \quad \text{with} \quad k \in \{0,1\}. \tag{2}$$

We have chosen our coordinate system along the cubic axes, where z is the growth direction of the QDs. In figures 2(a) and (b), respectively, we present contour plots of $|F^{(1;3/2,-3/2)}(E,\vec{r})|^2$ and $|F^{(1;3/2,-1/2)}(E,\vec{r})|^2$ in the $x = 0$ plane. The corresponding coordinate system is depicted in figure 1(a).

The energy difference between $|\Psi_1\rangle$ and the next higher energy eigenstate $|\Psi_2\rangle$ is larger than 1 meV, versus a splitting of $\approx 0.4\,\mu$eV between the lowest two states. Hence, the system near the ground state is well described by a two-level system with basis states $|\Psi_0\rangle$ and $|\Psi_1\rangle$. These are essentially linear combinations of upper- and lower-dot hole states, with the admixture depending on the value of the external electric field. The effective Hamiltonian of the pseudo-spin system reads [21]

$$H_0 = \frac{\mu_B}{2}\vec{\sigma} \cdot g(E) \cdot \vec{B}, \tag{3}$$

where $\vec{\sigma}$, $g(E)$ and $\vec{B}$, respectively, denote the Pauli matrix vector of the pseudo-spin-$\frac{1}{2}$ system, the electrically tunable hole g tensor and the externally applied magnetic field. Note that

(a) $|F^{(1;3/2,-3/2)}(E,\vec{r})|^2$ (b) $|F^{(1;3/2,-1/2)}(E,\vec{r})|^2$
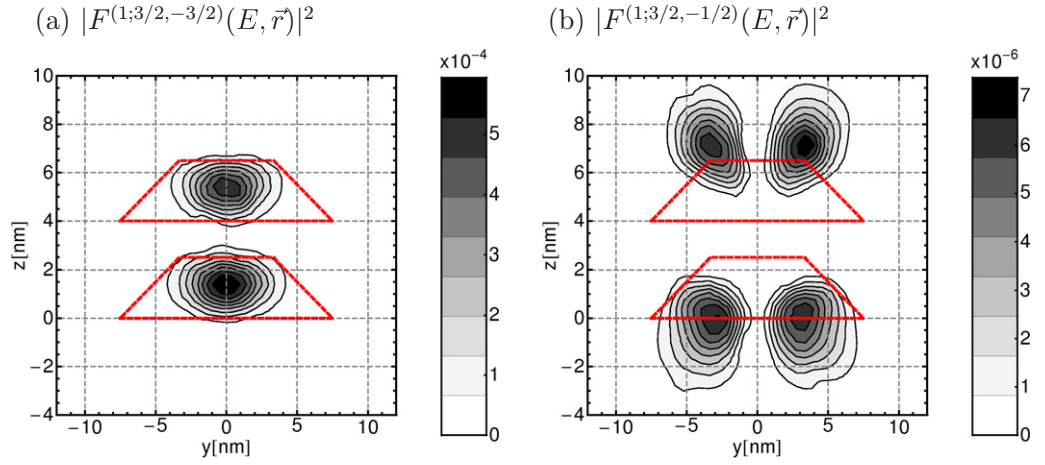
Figure 2. Spatial dependence of the envelope functions $|F^{(1;3/2;j_z)}(E,\vec{r})|^2$ within the $x=0$ plane (see figure 1(a)) for (a) the hh contribution with $j_z=-3/2$ and (b) for the lh contribution with $j_z=-1/2$. All envelope functions are given for $E=0\,\mathrm{kV\,cm^{-1}}$ and $\vec{B}=(0,0,10)\,\mathrm{mT}$. The cross-sections of the pyramidal QDs are indicated by red dashed lines.

equation (3) is given in the basis $\{|\Psi_1\rangle, |\Psi_0\rangle\}$. By choosing a constant magnetic field of the form $\vec{B}=(B,-B,B)$, equation (3) takes the form

$$H_0 = \frac{\mu_B}{2}\vec{\sigma}\begin{bmatrix} \frac{g^{110}+g^{1\bar{1}0}}{2} & \frac{g^{110}-g^{1\bar{1}0}}{2} & 0 \\ \frac{g^{110}-g^{1\bar{1}0}}{2} & \frac{g^{110}+g^{1\bar{1}0}}{2} & 0 \\ 0 & 0 & g^{001} \end{bmatrix}\begin{bmatrix} B \\ -B \\ B \end{bmatrix} = \frac{\mu_B}{2}B[(\sigma_x-\sigma_y)g^{1\bar{1}0}+g^{001}\sigma_z]. \tag{4}$$

Throughout this paper, we choose a value of $B=10\,\mathrm{mT}$ and an external electric field pointing along the [001] direction, $\vec{E}=(0,0,E)$. A non-vanishing in-plane magnetic field is necessary in order to obtain full control over the qubit.

2.1. Hole–nuclear-spin interaction

In addition to the externally applied magnetic field, the hole experiences an effective magnetic field that results from the nuclear spins of the host lattice. This is a consequence of the non-vanishing dipole–dipole hyperfine interaction (in contrast to the Fermi contact hyperfine interaction that vanishes for wavefunctions of p-symmetry), as well as the coupling of the hole orbital angular momentum to the nuclear spins [14, 15]. We now determine this effective field.

The corresponding interaction Hamiltonian of a single nuclear spin with a hole has the form [24]

$$H_I^i = 2\mu_B\gamma_i\vec{I}^i\cdot\left[\frac{\vec{l}^i}{\rho_i^3}-\frac{\vec{s}}{\rho_i^3}+\frac{3\vec{\rho}_i(\vec{s}\cdot\vec{\rho}_i)}{\rho_i^5}\right], \tag{5}$$

where $\vec{I}^i$ denotes the ith nuclear-spin operator and γ_i and μ_B, respectively, denote the gyromagnetic ratio of the ith nuclear spin and the Bohr magneton. The hole spin operator

is denoted by $\vec{s}$, $\vec{\rho}_i = \vec{r} - \vec{R}_i$ is the distance vector between the hole and the ith nuclear spin (located at $\vec{R}_i$), and $\vec{l}^i = \vec{\rho}_i \times \vec{p}$ denotes the hole orbital angular momentum operator. We note that $\vec{r}$ and $\vec{R}_i$ are given in the coordinate system introduced in figures 1(a) and 2(a) and (b). The matrix elements of H_I are now calculated in the $\{|\Psi_0\rangle, |\Psi_1\rangle\}$ basis defined above. We closely follow the approach given in [13, 15] and obtain

$$\langle \Psi_k | H_I^i | \Psi_l \rangle \equiv \sum_{j_z, j_z'} [F^{(k; \frac{3}{2}, j_z')}(E, \vec{R}_i)]^* F^{(l; \frac{3}{2}, j_z)}(E, \vec{R}_i) V_{j_z', j_z}^i. \tag{6}$$

The matrix elements with respect to the four basis functions $\{\psi^{(\frac{3}{2}, \frac{3}{2})}, \psi^{(\frac{3}{2}, \frac{1}{2})}, \psi^{(\frac{3}{2}, -\frac{1}{2})}, \psi^{(\frac{3}{2}, -\frac{3}{2})}\}$ are given by[4]

$$V_{j_z', j_z}^i \equiv c_i \begin{bmatrix} I_z^i & \frac{1}{\sqrt{3}} I_-^i & 0 & 0 \\ \frac{1}{\sqrt{3}} I_+^i & \frac{1}{3} I_z^i & \frac{2}{3} I_-^i & 0 \\ 0 & \frac{2}{3} I_+^i & -\frac{1}{3} I_z^i & \frac{1}{\sqrt{3}} I_-^i \\ 0 & 0 & \frac{1}{\sqrt{3}} I_+^i & -I_z^i \end{bmatrix}, \tag{7}$$

where $I_\pm^i = I_x^i \pm I_y^i$ and I_z^i are the nuclear-spin operators and

$$c_i = \frac{8\mu_B \gamma_i \hbar \Omega}{5} \int_0^{R_0} d\rho \frac{|\kappa(\rho)|^2}{\rho}. \tag{8}$$

The integration in equation (8) extends over the dominant part of the interaction defined by a radius R_0 around the nuclear spin under consideration and $\kappa(\rho)$ is the radial part of the basis functions. The details of the calculation are given in appendix A. Finally, the interaction of the ensemble of nuclear spins with the two-level system can be cast into the form

$$H_{nuc}(\vec{B}_n) = \sum_i H_I^i = \frac{\mu_B}{2} \vec{\sigma} \cdot \vec{B}_n, \tag{9}$$

where i runs over all $N \approx 10^4$–10^5 nuclear spins interacting with the hole. This has the form of the interaction of the pseudo-spin with an effective operator-valued magnetic field $\vec{B}_n$. The dynamics of the hole is much faster than that of the nuclear spins. This allows one to employ a quasi-static approximation for $\vec{B}_n$ for the time period of a single measurement (initialization, manipulation and readout) of the hole spin qubit so that $\vec{B}_n$ may be approximated by a classical constant vector [3, 4, 25]. During the time it takes to perform 10^3–10^4 repetitions of the measurement, the effective nuclear magnetic field varies significantly, leading to inhomogeneous-broadening-type dynamics [25]. The simplest way to take into account this variation is to treat the vector components of $\vec{B}_n = (B_n^x, B_n^y, B_n^z)$ as random variables with Gaussian probability distributions [3, 4, 25]

$$P(\vec{B}_n) = P(B_n^x) P(B_n^y) P(B_n^z) \quad \text{with} \quad P(B_n^i) = \frac{1}{\sqrt{2\pi} \Delta_i} \exp\left[-(B_n^i)^2/(2\Delta_i^2)\right]. \tag{10}$$

Here, $P(B_n^i)$ is the probability of finding a value B_n^i for the effective nuclear magnetic field along the i-direction and $\Delta_i^2 \equiv \langle B_n^i B_n^i \rangle - \langle B_n^i \rangle^2$ denotes the corresponding variance of the effective

---

[4] Note that we find positive signs for the matrix elements $V_{1/2, -1/2}^i$ and $V_{-1/2, 1/2}^i$ in contrast to [15].

magnetic field fluctuation. We assume an 'infinite temperature' nuclear-spin density matrix, i.e. $\rho_n = (2I + 1)^{-N} \mathbb{1}$ [4]. Hence, the mean values $\langle B_n^i \rangle$ vanish for all directions i. Furthermore, we assume that the spin bath is uncorrelated, i.e. $\langle B_n^i B_n^j \rangle = 0$ for $i \neq j$. Finally, the total Hamiltonian of the system reads

$$H(\vec{B}_n) = H_0 + H_{nuc}(\vec{B}_n). \tag{11}$$

We note that $H(\vec{B}_n)$ is time dependent via the electric field that is applied to control the hole dynamics.

In a recent experiment, the dephasing time of a hole spin in a single QD has been determined to be at least $T_{2,h}^* \approx 100$ ns [16]. This corresponds to a variance of $\Delta_z = \hbar/(\mu_B T_{2,h}^*) \approx 0.1$ mT [25]. We use this value for our simulation of the hole–nuclear-spin interaction. The variances Δ_x and Δ_y are calculated in appendix B. We find that $\Delta_x/\Delta_z \approx \Delta_y/\Delta_z \approx 10^{-1}$.

2.2. Hole–phonon interaction

The coupling of the hole to acoustic phonons via the piezoelectric and deformation potential interactions leads to additional dephasing and relaxation [26]. To account for these mechanisms, we employ a Lindblad model [27]. The dissipator reads

$$\mathcal{D}[\rho] = \Gamma_\downarrow \left[\sigma_- \rho \sigma_+ - \frac{1}{2} \{ \sigma_+ \sigma_-, \rho \} \right] + \Gamma_\uparrow \left[\sigma_+ \rho \sigma_- - \frac{1}{2} \{ \sigma_- \sigma_+, \rho \} \right] + \frac{\Gamma_{ph}^\Phi}{2} \left[\sigma_z \rho \sigma_z - \rho \right], \tag{12}$$

with $\Gamma_\downarrow$, $\Gamma_\uparrow$ and Γ_{ph}^Φ denoting the relaxation rates for the transitions $|\Psi_1\rangle \rightarrow |\Psi_0\rangle$, $|\Psi_0\rangle \rightarrow |\Psi_1\rangle$ and the pure dephasing rate, respectively. The braces denote anticommutators. For simplicity, we set $\Gamma_{ph}^\Phi = \Gamma_\uparrow = \Gamma_\downarrow \equiv \Gamma$. The range of reported relaxation times varies significantly with temperature and the externally applied magnetic field [28, 29]. For this work, we choose a relatively conservative value of $T_{1,h} = 1\,\mu s = 1/(\Gamma_\uparrow + \Gamma_\downarrow) = 1/\Gamma$. We note that the hole relaxation rate for QDs due to phonon interaction does not increase with decreasing external magnetic field [12, 26, 28, 30].

2.3. Hole-spin dynamics

Inspection of figure 1(b) reveals that the g tensor component $g^{001}(E)$ cannot be tuned to 0, in contrast to $g^{1\bar{1}0}(E)$. For a simpler description of the hole-spin dynamics, it is therefore useful to switch to a rotating frame $|\psi\rangle \rightarrow |\tilde{\psi}\rangle \equiv U_2 |\psi\rangle$, which rotates around the z-axis with a frequency given by

$$\omega^* = \mu_B g^{001}(E^*) B/\hbar. \tag{13}$$

The transformation is characterized by the time-dependent unitary operator $U_2 \equiv \exp(i\omega^* t \sigma_z/2)$, where the electric field E^* is defined by the relation

$$g^{1\bar{1}0}(E^*) = 0. \tag{14}$$

In addition, we perform another *time-independent* rotation $U_1 = e^{-i(\pi/8)\sigma_z}$, which corresponds to the pseudo-spin rotation $\sigma_x - \sigma_y \rightarrow \sqrt{2}\sigma_x$ in equation (4). In this rotating coordinate system

(labeled by a tilde), the Lindblad equation for the density matrix reads

$$\tilde{\rho}(\vec{B}_n, t) = U_2 U_1 \rho(\vec{B}_n, t) U_1^\dagger U_2^\dagger,$$

$$\frac{d\tilde{\rho}(\vec{B}_n, t)}{dt} = -\frac{i}{\hbar}[H_r(\vec{B}_n), \tilde{\rho}(\vec{B}_n, t)] + \tilde{\mathcal{D}}[\tilde{\rho}(\vec{B}_n, t)], \tag{15}$$

$$H_r(\vec{B}_n) = U_2 U_1 H(\vec{B}_n) U_1^\dagger U_2^\dagger + i\hbar \frac{dU_2}{dt} U_2^\dagger,$$

with $H(\vec{B}_n)$ given in equation (11). It can be shown that $\tilde{\mathcal{D}}[\tilde{\rho}(\vec{B}_n, t)] = \mathcal{D}[\tilde{\rho}(\vec{B}_n, t)]$, i.e. the form of the dissipator is invariant under the coordinate transformations described above. The density matrix has to be averaged over the effective nuclear magnetic field $\vec{B}_n$ of each measurement. It is calculated by averaging over typically $M = 3000$ values of the random effective nuclear magnetic field with probability distributions as given in equation (10), using

$$\tilde{\rho}(t) = (1/M) \sum_M \tilde{\rho}(\vec{B}_n). \tag{16}$$

3. Results

3.1. Pulse shape optimization

In the previous section, we have detailed the hole-spin qubit and identified a complete control mechanism. We are now in a position to find optimal electric fields that perform any type of qubit transformation. However, the dependence of the g tensor elements on the electric field E is a complex one, as can be seen in figure 1(b). Therefore, appropriate control fields can, in general, not be determined analytically, particularly, if the finite rise time of the electric control is to be taken into account. Here, we apply optimal control theory in order to determine both realistic and simple pulse shapes.

We start by outlining how to characterize qubit operations. For single-qubit systems, quantum gate transformations can be described as rigid rotations of the Bloch sphere. For unitary dynamics, this rotation can be fully described by the time evolution propagator $U(t)$ corresponding to the Hamiltonian $H_r(\vec{B}_n)$ given in equation (15). However, it is more advantageous to employ the so-called process tomography matrix (PTM) $\chi(t)$. For strictly unitary dynamics, this matrix takes the simple form [31]

$$\chi(t) = U(t)^* \otimes U(t), \tag{17}$$

with $U(t)^*$ denoting the complex conjugate of the matrix representation of $U(t)$. The PTM eliminates physically irrelevant global phases of the propagator $U \to e^{i\Phi} U$, can be readily obtained in experiments [32]–[34] and can be employed for non-unitary dynamics as well [35, 36].

The next step is to define a cost functional that quantitatively reflects how accurately a control field achieves a given unitary gate transformation. We use the PTM of equation (17) that implicitly depends on the electric field, $\chi(t) = \chi[E(t); t]$, and seek electric pulse shapes that minimize the following cost functional [37]:

$$J[E] = \text{tr}\left\{ [\chi(t_f) - \chi_D][\chi(t_f) - \chi_D]^\dagger \right\}, \tag{18}$$

where χ_D denotes the ideal PTM and the interval $(0, t_f)$ is the time span allowed for the gate transformation (gate operation time). A perfect implementation of the given unitary gate transformation corresponds to $J = 0$. Other distance measures for open quantum systems are given in [38]–[42]. We choose the following analytic form of the electric control field:

$$E(t) = E^* + \sum_{j=1}^{M} \frac{A_j}{4} \left\{ 1 + \tanh \left[\alpha \left(t - \sum_{i=1}^{j} \Delta t_i \right) \right] \right\} \left\{ 1 + \tanh \left[\alpha \left(\sum_{i=1}^{j} \Delta t_i - t \right) \right] \right\}, \quad (19)$$

where A_j and Δt_j are the parameters to be optimized and E^* is the working point defined by equation (14). The pulse form of equation (19) corresponds to a sequence of M voltage steps of amplitude A_j, each of duration Δt_j. The finite rise time of the pulses is determined by the parameter α that we set to $\alpha = 8.79 \, \text{ns}^{-1}$. The optimal control field $E_{\text{opt}}(t)$ is obtained from the minimization procedure

$$J_{\text{opt}}[E_{\text{opt}}] = \min_{\{A_j, \Delta t_j\}} J[E(A_j, \Delta t_j)]. \quad (20)$$

We then use the optimal control field $E(t) = E_{\text{opt}}(t)$ to determine the PTM with dephasing and relaxation included in our simulations. We note that, in the non-unitary case, $\chi(t)$ is no longer given by equation (17) but can be computed by using equations (15) (see [37] for details of this calculation). However, the form of the cost functional given in equation (18) does not change. Thus, a value $J > 0$ reflects suboptimal pulse shaping and/or the presence of decoherence and relaxation effects. In addition to J, it is customary to define a fidelity loss of the gate operation by

$$\Delta F[E] = (J[E] / J_{\text{max}})^{1/2}, \quad (21)$$

with $J_{\text{max}} = 2n^2$, where n denotes the number of basis states of the quantum system, i.e. $n = 2$ for single qubits. A perfect execution of the gate operation corresponds to $\Delta F[E] = 0$. For brevity, we will write ΔF instead of $\Delta F[E]$ throughout this work.

We perform the cost functional minimization (equation (20)) for both the Hadamard operation (which transforms the axes of the Bloch sphere as follows: $x \to z$, $z \to x$ and $y \to -y$) and a $\pi/2$ rotation around the y-axis. The corresponding unitary evolution operators U_{H} and $U_{\pi/2}$ and the ideal PTM χ_{H} and $\chi_{\pi/2}$, respectively, read (see equation (17))

$$U_{\text{H}} = \frac{1}{\sqrt{2}} \begin{bmatrix} 1 & 1 \\ 1 & -1 \end{bmatrix}, \quad U_{\pi/2} = \frac{1}{\sqrt{2}} \begin{bmatrix} 1 & -1 \\ 1 & 1 \end{bmatrix},$$

$$\chi_{\text{H}} = (U_{\text{H}})^* \otimes U_{\text{H}}, \quad \chi_{\pi/2} = (U_{\pi/2})^* \otimes U_{\pi/2}.$$

We set the gate operation time $t_f = 10 \, \text{ns}$. The minimization is executed within a differential evolution algorithm [43]. For the Hadamard gate, the algorithm converges to an optimal control field that consists of three pulses, depicted in figure 3(a). The $\pi/2$ rotation, on the other hand, is realized by an optimal control field consisting of four pulses, as shown in figure 3(c). Trajectories of the Bloch vector for both transformations with equal initial states (Ψ_1) are given in figures 3(b) and (d).

If we do not account for decoherence and relaxation in our simulations, the fidelity losses due to imperfect pulse shaping are of the order $\Delta F \approx 0.001\%$. When decoherence and relaxation are included, the fidelity loss increases to $\Delta F \approx 1\%$, which gives excellent

IOP Institute of Physics **Φ** DEUTSCHE PHYSIKALISCHE GESELLSCHAFT
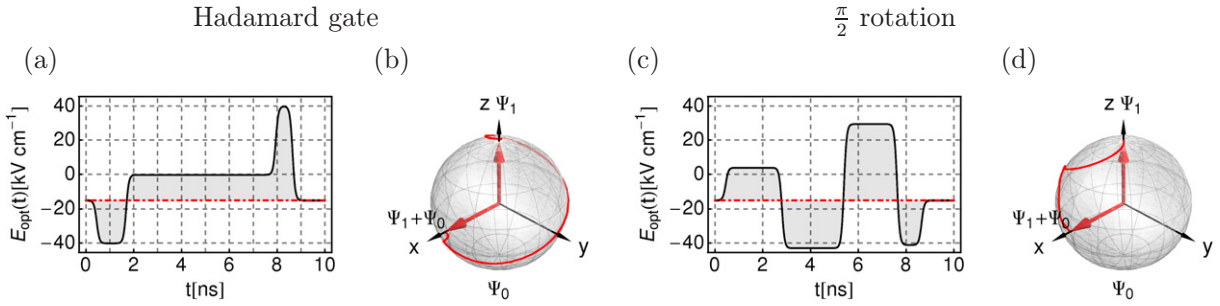
Figure 3. (a) Optimal electric pulse shape $E_{opt}(t)$ for the Hadamard transformation and (c) for the $\pi/2$ rotation. The dot-dashed red lines correspond to $E = E^*$ given in equation (14). (b) The trajectory of the Bloch vector for the Hadamard gate and (d) for the $\pi/2$ pulse. The final states of both transformations coincide for the initial state Ψ_1, although the trajectories of the Bloch vectors differ.
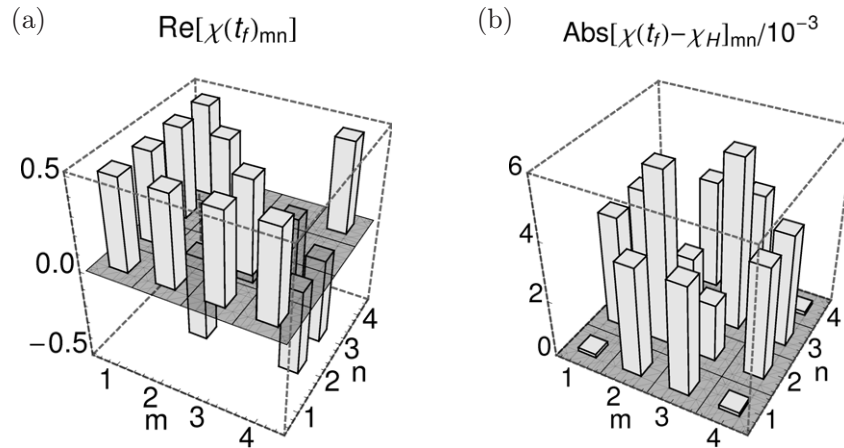

Figure 4. (a) Real part of the matrix elements (m, n) of the optimal Hadamard PTM $\chi(t_f)$. (b) Deviation of the optimal PTM with respect to χ_H (relaxation and dephasing included). The corresponding fidelity loss is $\Delta F \approx 1\%$.

performance. The contributions to the fidelity loss due to phonons and nuclear spins are approximately of the same order. For the Hadamard gate, the real parts of the matrix elements (m, n) of the optimal PTM, $Re[\chi(t_f)_{mn}]$, as well as the deviation of the optimal PTM from the ideal PTM χ_H, are shown in figures 4(a) and (b), respectively.

3.2. Hole-spin echo

It is frequently important to analyze the characteristics of dephasing processes of a quantum system that are not associated with inhomogeneous dephasing, such as caused by the hole–nuclear-spin interaction discussed in section 2.1 in the present case. This can be achieved with spin-echo experiments [44]. The decay of the peak value of the spin-echo recovery signal gives information about the additional cumulative dephasing rate and the time dependence of the coherence loss (e.g. exponential versus polynomial decay).

(a)

(b) $\mathrm{Re}[\tilde{\rho}_{01}(t)]$

(c) $\mathrm{Abs}[\tilde{\rho}_{01}(t)]$
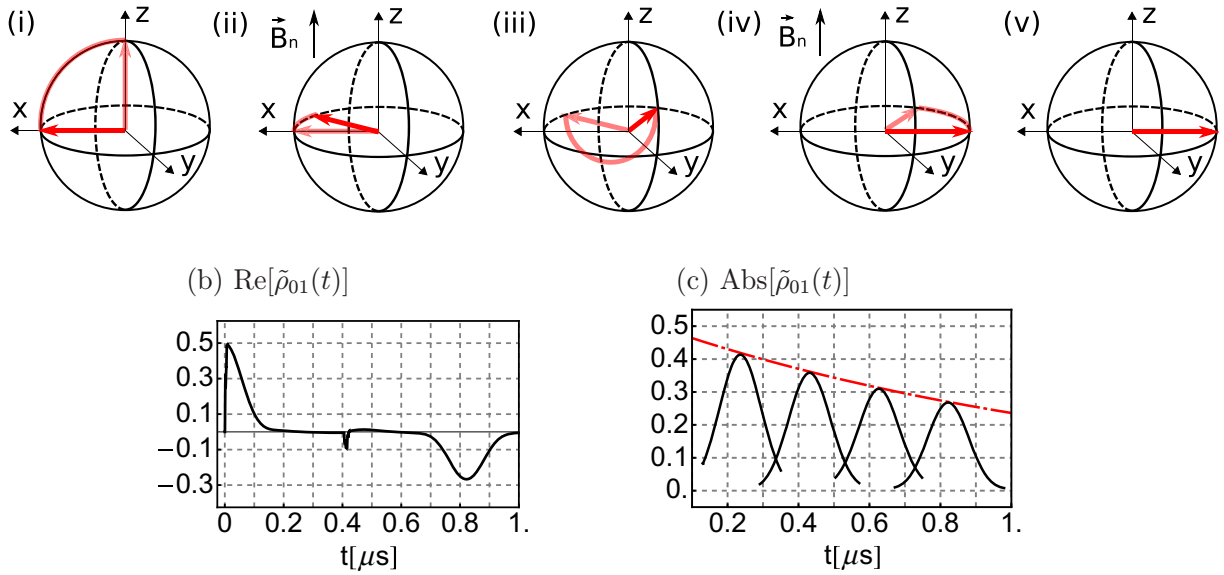
Figure 5. (a) Schematic spin-echo sequence as described in the main text. The red (dark gray) arrow denotes the Bloch vector. (b) Time dependence of the coherence $\mathrm{Re}[\tilde{\rho}_{01}(t)]$. The spike at $t \approx 0.4\,\mu\mathrm{s}$ is a consequence of the π-pulse. At $t \approx 0.8\,\mu\mathrm{s}$, a partial revival of coherence can be observed. (c) The solid black lines denote spin-echo signals for different pulse separation times t_1. The decrease of the peak echo signal is denoted by the red dot-dashed line.

In figure 5(a), we show the crucial steps that are needed to perform a spin-echo experiment for the hole-spin qubit.

(i) At time $t = 0$, one applies a $\pi/2$ pulse such as given in figure 3(c). It transforms the initial qubit state $|\Psi_1\rangle$ into the superposition state $1/\sqrt{2}\,(|\Psi_0\rangle + |\Psi_1\rangle)$ [44].

(ii) Subsequently, the Bloch vector of the qubit evolves according to the system dynamics, including dissipation, decoherence and the effective magnetic field from the nuclear spins. The latter causes a rotation of the Bloch vector around a random axis, given by the direction of $\vec{B}_\mathrm{n}$.

(iii) At time $t_1 > 0$, one applies a π pulse that is composed of two subsequent $\pi/2$ pulses. It rotates the Bloch vector by an angle π around the y-axis of the Bloch sphere.

(iv) Next, the Bloch vector evolves again.

(v) At time $t = 2t_1$, the coherence, represented by $\mathrm{Re}[\tilde{\rho}_{01}(t)]$, is partly restored.

Here, $\tilde{\rho}_{01}(t)$ is the off-diagonal matrix element of the density matrix $\tilde{\rho}(t)$ in the pseudo-spin basis (see equation (16)) and serves as a measure for coherence. For $t_1 \approx 0.4\,\mu\mathrm{s}$, a plot of its time evolution during a spin-echo experiment, as obtained within our model, is shown in figure 5(b). Spin-echo signals corresponding to different pulse separation times t_1 are given in figure 5(c). Since relaxation and pure dephasing due to the spin–phonon interaction are included in our simulation, the restoration of coherence is obtained as imperfect. The peak values of the echoes decrease approximately as $\sim \exp\{-2t_1[(\Gamma_\uparrow + \Gamma_\downarrow)/2 + \Gamma_\mathrm{ph}^\Phi]\}$, indicated by the red dot-dashed line
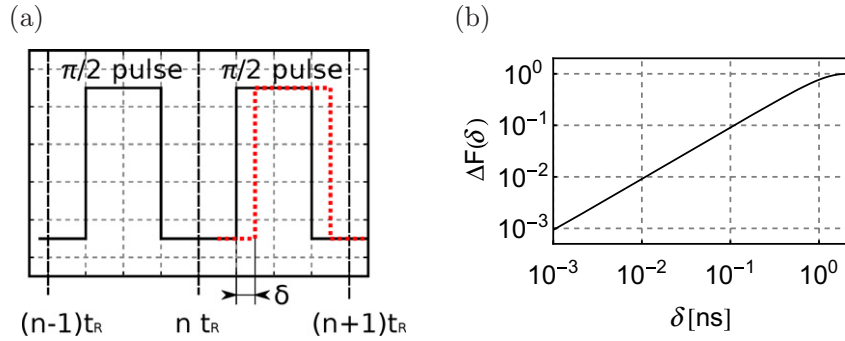
Figure 6. (a) The schematic ideal pulse sequence is denoted by the black solid line. The second imperfect $\pi/2$ pulse (red/gray dashed line) is delayed by δ. (b) Double logarithmic plot of the fidelity loss ΔF versus the delay time error δ.

in figure 5(c). We note that the non-vanishing transversal nuclear magnetic field components B_n^x and B_n^y can also lead to a reduction of the peak value of the echo signal. However, we have analyzed this effect and, for the present system, have found the spin-echo signal due to longitudinal contributions and that due to longitudinal and transversal contributions (such as given in figures 5(b) and (c)) to be congruent.

3.3. Pulse timing imperfections

As mentioned above, the π-pulse of the proposed spin-echo sequence is composed of two subsequent $\pi/2$ pulses. Due to the form of the Hamiltonian in equation (15), these composite pulses should be applied at special times (integer multiples of $t_R = 2\pi/\omega^*$ after state initialization) in order to preserve the high fidelity of the gate transformation. This requirement is due to the effective magnetic field $g(E) \cdot \vec{B}$ along the z-direction that cannot be tuned to zero by electric means. The dependence of the fidelity loss ΔF with respect to a pulse delay time error δ between two subsequent $\pi/2$-pulses is shown in figure 6. This figure illustrates that the additional fidelity loss ΔF is smaller than 1% as long as $\delta \leqslant 10\,\mathrm{ps}$, which should be readily within the reach of present-day experiments. The sensitivity to the delay time error can be further decreased by reducing the magnitude of the external magnetic field.

4. Summary

We propose a qubit realization in the form of the spin of a hole in a QDM, which is controlled all-electrically by g tensor modulation, and evaluate its performance regarding controllability and dissipative effects. The growth of InAs/GaAs QDMs and the electric control of excitonic g tensors have already been demonstrated in the laboratory [19]. An effective qubit model for such a QDM is derived from a detailed electronic structure calculation, as well as from the inclusion of the interaction with nuclear spins of the host lattice and phonons. In [21], the methods of this electronic structure calculation have been used to describe the g tensor modulation observed in [19] and have shown excellent agreement with the experiment. On the basis of the effective qubit model, we predict that high-fidelity gate operations for a single hole within a QDM are experimentally feasible and promising.

The qubit can be fully controlled by means of an external electric field E that leads to a change of the effective magnetic field $g(E) \cdot \vec{B}$. In the present work, a constant magnetic field of the order of $|\vec{B}| \approx 10\,\mathrm{mT}$ leads to a moderate time scale of the qubit dynamics and therefore ensures the experimental feasibility of the qubit control. We use optimal control methods in order to determine simple electric control pulses, as illustrated for the Hadamard gate and for a $\pi/2$ qubit rotation around the y-axis of the Bloch sphere. The 10 ns pulse profiles consist of voltage steps with a finite rise time that can be generated in experiment by arbitrary waveform generators. The performance of the gate transformations is tested with respect to dephasing and relaxation due to the interaction of the hole spin with the surrounding nuclear spins of the host lattice and due to the hole–phonon interaction. For electric pulses of duration 10 ns, we find that qubit manipulations can be performed with a remarkably low fidelity loss of $\Delta F \approx 1\%$.

We propose a spin-echo experiment that allows one to completely cancel inhomogeneous dephasing due to the hole–nuclear-spin interaction. Therefore, it would enable the experimenter to study and characterize additional dephasing mechanisms beyond inhomogeneous broadening. We also investigate the influence of pulse-timing imperfections on the gate fidelity. Our findings show that the additional fidelity loss is $\lesssim 1\%$ for pulse delay time errors of less than 10 ps.

Acknowledgments

Appendix A. Matrix elements of the hole–nuclear-spin Hamiltonian

In this section, we derive the matrix elements of equation (6). For simplicity, we omit the nuclear spin index i. The interaction Hamiltonian of a nuclear spin $\vec{I}$ (located at $\vec{R}$) with a hole reads (see section 2.1 and [24]),

$$H_{\mathrm{I}}(\vec{\rho}, \vec{p}) = 2\mu_{\mathrm{B}}\gamma \vec{I} \cdot \left[\frac{\vec{l}}{|\rho|^3} - \frac{\vec{s}}{|\rho|^3} + \frac{3\vec{\rho}\,(\vec{s}\cdot\vec{\rho})}{|\rho|^5} \right] \tag{A.1}$$

$$= 2\mu_{\mathrm{B}}\gamma I_m \otimes \left[\left(\frac{l_m}{|\rho|^3} \otimes \mathbb{1} \right) - \left(\frac{\rho^2 \delta_{mn} - 3\rho_m \rho_n}{|\rho|^5} \right) \otimes s_n \right], \tag{A.2}$$

where we used the Einstein summation convention for the indices m and n. Here γ, $\vec{s}$ and $\vec{l} = \vec{\rho} \times \vec{p}$, respectively, denote the gyromagnetic ratio of the nuclear spin $\vec{I}$, the hole spin and the hole orbital angular momentum. In equation (A.1), we explicitly denoted the spatial and momentum dependence of H_{I}. The hole wave function Ψ can be written as a product of envelope functions F and angular-momentum basis functions $\psi^{(j,j_z)}$,

$$\Psi_k(\vec{r}) = \sqrt{\Omega} \sum_{j,j_z} F^{(k;j,j_z)}(E, \vec{r}) \psi^{(j,j_z)}(\vec{r}), \quad j_z \in \left\{ \pm\frac{3}{2}, \pm\frac{1}{2} \right\}, \quad j \in \left\{ \frac{3}{2}, \frac{1}{2} \right\}, \quad k \in \{0, 1\}, \tag{A.3}$$

or, using spin-resolved zone center valence-band Bloch functions $\psi^{(i,\alpha)}$, as

$$\Psi_k(\vec{r}) = \sqrt{\Omega} \sum_{i,\alpha} F^{(k;i,\alpha)}(E, \vec{r}) \psi^{(i,\alpha)}(\vec{r}), \quad i \in \{X, Y, Z\}, \quad \alpha \in \{\uparrow, \downarrow\}, \quad k \in \{0, 1\}. \tag{A.4}$$

The matrix that describes the transformation between $\psi^{(j,j_z)}$ and $\psi^{(i,\alpha)}$ is given in equation (A.8) [23, 45]. The wavefunctions $\Psi_0(\vec{r})$ and $\Psi_1(\vec{r})$ denote the ground and the first excited Zeeman state of the QDM. We neglect states with higher energy (see section 2) and calculate the matrix elements of the interaction Hamiltonian

$$H_{\mathrm{I}}(\vec{\rho}, \vec{p}) = \begin{bmatrix} \langle \Psi_1 | H_{\mathrm{I}}(\vec{\rho}, \vec{p}) | \Psi_1 \rangle & \langle \Psi_1 | H_{\mathrm{I}}(\vec{\rho}, \vec{p}) | \Psi_0 \rangle \\ \langle \Psi_0 | H_{\mathrm{I}}(\vec{\rho}, \vec{p}) | \Psi_1 \rangle & \langle \Psi_0 | H_{\mathrm{I}}(\vec{\rho}, \vec{p}) | \Psi_0 \rangle \end{bmatrix}, \tag{A.5}$$

with

$$\langle \Psi_k | H_{\mathrm{I}}(\vec{\rho}, \vec{p}) | \Psi_l \rangle = \Omega \sum_{i,j,\alpha,\beta} \int_V \mathrm{d}\vec{\rho}\,\mathrm{d}\vec{\tau} \{ [F^{(k;i,\alpha)}(E, \vec{\tau} + \vec{R}) \psi^{(i,\alpha)}(\vec{\tau} + \vec{R})]^*$$

$$\times \langle \vec{\tau} | H_{\mathrm{I}}(\vec{\rho}, \vec{p}) | \vec{\rho} \rangle \, \psi^{(j,\beta)}(\vec{\rho} + \vec{R}) F^{(l;j,\beta)}(E, \vec{\rho} + \vec{R}) \},$$

where $\vec{R}$ denotes the position of the nuclear spin with respect to the coordinate system given in figures 1(a) and 2(a) and (b) and with $\vec{\tau} = \vec{r} - \vec{R}$ denoting a spatial coordinate. Since the hole–nuclear-spin interaction is short ranged, we can assume that it is non-vanishing only within a sphere of volume V_{R_0} and radius R_0 around the nuclear spin [13]. Furthermore, the envelope functions are approximately constant within this sphere, i.e.

$$\langle \Psi_k | H_{\mathrm{I}}(\vec{\rho}, \vec{p}) | \Psi_l \rangle$$

$$\approx \Omega \sum_{i,j,\alpha,\beta} [F^{(k;i,\alpha)}(E, \vec{R})]^* F^{(l;j,\beta)}(E, \vec{R}) \int_{V_{R_0}} \mathrm{d}\vec{\rho} \left[\psi^{(i,\alpha)}(\vec{\rho}) \right]^* H_{\mathrm{I}}(\vec{\rho}, -\mathrm{i}\hbar \vec{\nabla}_{\vec{\rho}}) \psi^{(j,\beta)}(\vec{\rho}),$$

$$\equiv \sum_{i,j,\alpha,\beta} [F^{(k;i,\alpha)}(E, \vec{R})]^* F^{(l;j,\beta)}(E, \vec{R}) V_{ij\alpha\beta}, \tag{A.6}$$

where we used the spatial periodicity of $\psi^{(i,\alpha)}(\vec{\rho})$ and $\langle \vec{\tau} | H_{\mathrm{I}}(\vec{\rho}, \vec{p}) | \vec{\rho} \rangle = H_{\mathrm{I}}(\vec{\rho}, -\mathrm{i}\hbar \vec{\nabla}_{\vec{\rho}}) \delta(\vec{\rho} - \vec{\tau})$. In fact, it can be shown that V_{R_0} is well approximated by the unit cell around the nuclear spin under consideration. Contributions due to long range interactions lead to corrections of the order of 1% [14, 15]. Following [13], we employ a spherical approximation of the basis functions $\psi^{(i,\alpha)}(\vec{\rho})$. Using spherical coordinates (ρ, θ, ϕ), the corresponding approximate basis functions read

$$\psi^{(X,\alpha)}(\rho, \theta, \phi) \approx \sqrt{\frac{3}{4\pi}} \kappa(\rho) \sin(\theta) \cos(\phi) |\alpha\rangle,$$

$$\psi^{(Y,\alpha)}(\rho, \theta, \phi) \approx \sqrt{\frac{3}{4\pi}} \kappa(\rho) \sin(\theta) \sin(\phi) |\alpha\rangle,$$

$$\psi^{(Z,\alpha)}(\rho, \theta, \phi) \approx \sqrt{\frac{3}{4\pi}} \kappa(\rho) \cos(\theta) |\alpha\rangle.$$

Here, $\kappa(\rho)$ denotes the radial part of $\psi^{(i,\alpha)}(\rho, \theta, \phi)$ and $|\alpha\rangle$ is a ket in the spin basis $\{\uparrow, \downarrow\}$. An estimation of the magnitude of the hole–nuclear-spin interaction is given in [14], where the authors used a linear combination of atomic orbitals for the hh Bloch function. In the

basis $\psi^{(i,\alpha)}$ [$\alpha, \beta \in \{\uparrow, \downarrow\}$ and $i, j \in \{X, Y, Z\}$] and by employing the aforementioned spherical approximation, the integral $V_{ij\alpha\beta}$ (equation (A.6)) can be expressed as

$$\frac{V_{ij\alpha\beta}}{\Omega} = 2\mu_{\mathrm{B}}\gamma \, I_m \int_0^{R_0} \mathrm{d}\rho \frac{\kappa(\rho)^2}{\rho} \left[-\mathrm{i}\hbar\epsilon_{ijm}\delta_{\alpha\beta} - \frac{2}{5}\left(\delta_{ij}\delta_{mn} - \frac{3}{2}\left(\delta_{im}\delta_{jn} + \delta_{in}\delta_{jm} \right) \right) \langle\alpha| \, s_n \, |\beta\rangle \right]. \quad (A.7)$$

A discussion of modifications of the interaction at small ρ due to the finite size of the nucleus can be found in [46].

Since we want to express the hole–nuclear-spin interaction in terms of lh and hh contributions, we change the basis representation of $V_{ij\alpha\beta}$ from $\{\psi^{(i,\alpha)}\}$ to $\{\psi^{(j,j_z)}\}$. The transformation is governed by the unitary matrix [23, 45]

$$U_{\lambda\nu} = \frac{1}{\sqrt{6}} \begin{bmatrix} -\sqrt{3} & 0 & \mathrm{i}\sqrt{3} & 0 & 0 & 0 \\ 0 & -1 & 0 & \mathrm{i} & 2 & 0 \\ 1 & 0 & \mathrm{i} & 0 & 0 & 2 \\ 0 & \sqrt{3} & 0 & \mathrm{i}\sqrt{3} & 0 & 0 \\ 0 & -\sqrt{2} & 0 & \mathrm{i}\sqrt{2} & -\sqrt{2} & 0 \\ -\sqrt{2} & 0 & -\mathrm{i}\sqrt{2} & 0 & 0 & \sqrt{2} \end{bmatrix}, \quad (A.8)$$

where the new matrix representation $\tilde{V}$ is given by $\tilde{V}_{\mu\nu} = U_{\mu\sigma} V_{\sigma\lambda} U_{\lambda\nu}^\dagger$. Here, we use the shorthand notation

$$\begin{aligned} \mu, \nu = (j, j_z) &\in \left\{ \left(\tfrac{3}{2}, +\tfrac{3}{2}\right), \left(\tfrac{3}{2}, +\tfrac{1}{2}\right), \left(\tfrac{3}{2}, -\tfrac{1}{2}\right), \left(\tfrac{3}{2}, -\tfrac{3}{2}\right) \left(\tfrac{1}{2}, +\tfrac{1}{2}\right), \left(\tfrac{1}{2}, -\tfrac{1}{2}\right) \right\}, \\ \sigma, \lambda = (i, \alpha) &\in \left\{ (X, \uparrow), (X, \downarrow), (Y, \uparrow), (Y, \downarrow), (Z, \uparrow), (Z, \downarrow) \right\}. \end{aligned} \quad (A.9)$$

The transformed matrix $\tilde{V}_{\mu\nu}$ in the $\{\psi^{(3/2,+3/2)}, \psi^{(3/2,+1/2)}, \psi^{(3/2,-1/2)}, \psi^{(3/2,-3/2)}\}$ basis thus reads

$$\tilde{V}_{\mu\nu} = \frac{8\mu_{\mathrm{B}}\gamma\hbar\Omega}{5} \int_0^{R_0} \mathrm{d}\rho \frac{|\kappa(\rho)|^2}{\rho} \begin{bmatrix} I_z & \frac{1}{\sqrt{3}}I_- & 0 & 0 \\ \frac{1}{\sqrt{3}}I_+ & \frac{1}{3}I_z & \frac{2}{3}I_- & 0 \\ 0 & \frac{2}{3}I_+ & -\frac{1}{3}I_z & \frac{1}{\sqrt{3}}I_- \\ 0 & 0 & \frac{1}{\sqrt{3}}I_+ & -I_z \end{bmatrix} \equiv \bar{V}_{j_z', j_z}. \quad (A.10)$$

Split-off contributions ($j = \frac{1}{2}$) have been neglected as discussed in section 2. We finally arrive at the expression

$$\langle\Psi_k| H_{\mathrm{I}}(\vec{\rho}, \vec{p}) |\Psi_l\rangle \approx \sum_{j_z, j_z'} [F^{(k;j=3/2, j_z')}(E, \vec{R})]^* F^{(l;j=3/2, j_z)}(E, \vec{R}) \bar{V}_{j_z', j_z}, \quad (A.11)$$

for the $\{|\Psi_0\rangle, |\Psi_1\rangle\}$ matrix representation of the hole–nuclear-spin interaction (for the definition of $\bar{V}_{j_z', j_z}$ see equation (A.10)).

The Wigner–Eckart theorem can be used to determine the matrix elements of the hole–nuclear-spin interaction as well [47]–[49]. In addition to the calculation presented above, we decomposed the spatial part of equation (A.1) into spherical tensors $\tilde{l}_m$ and $\tilde{Q}_{mn}$,

$$l_m/\rho^5 \to \tilde{l}_m, \qquad \frac{\rho^2\delta_{mn} - 3\rho_m\rho_n}{\rho^5} \to \tilde{Q}_{mn}, \quad (A.12)$$

which correspond to angular momenta $j = 1$ and $j = 2$, respectively. The Wigner–Eckart theorem can then be readily applied to obtain the matrix elements in terms of Clebsch–Gordan

coefficients and so-called reduced matrix elements. However, in order to obtain a relation between the reduced matrix elements of the spherical tensors $\tilde{l}_m$ and $\tilde{Q}_{mn}$, approximations have to be employed as well. Hence, we decided to present the calculation of the matrix elements in terms of the spherical approximation given above.

Appendix B. Variances of the effective nuclear magnetic field

Here, we derive the expression for the effective nuclear magnetic field $\vec{B}_n$ given in equation (9), as well as the ratio of the variances Δ_x and Δ_y with respect to Δ_z (equations (10)). We rewrite equation (A.11) into

$$\langle \Psi_k | H_I(\vec{\rho}, \vec{p}) | \Psi_l \rangle = c[A_{kl}(E, \vec{R})I_+ + A_{kl}^\dagger(E, \vec{R})I_- + A_{kl}^z(E, \vec{R})I_z], \tag{B.1}$$

with $A(E, \vec{R})$, $A^\dagger(E, \vec{R})$ and $A^z(E, \vec{R})$ denoting 2×2 matrices and with c given in equation (8). The corresponding matrix elements read

$$A_{kl}(E, \vec{R}) = \tfrac{1}{3}\{\sqrt{3}[F^{(k;3/2,-1/2)}(\vec{R})]^* F^{(l;3/2,-3/2)}(\vec{R}) + 2[F^{(k;3/2,1/2)}(\vec{R})]^* F^{(l;3/2,-1/2)}(\vec{R})$$
$$+ \sqrt{3}[F^{(k;3/2,3/2)}(\vec{R})]^* F^{(l;3/2,1/2)}(\vec{R})\},$$

$$A_{kl}^z(E, \vec{R}) = \tfrac{1}{3}\{-3[F^{(k;3/2,-3/2)}(\vec{R})]^* F^{(l;3/2,-3/2)}(\vec{R}) - [F^{(k;3/2,-1/2)}(\vec{R})]^* F^{(l;3/2,-1/2)}(\vec{R})$$
$$+ [F^{(k;3/2,1/2)}(\vec{R})]^* F^{(l;3/2,1/2)}(\vec{R}) + 3[F^{(k;3/2,3/2)}(\vec{R})]^* F^{(l;3/2,3/2)}(\vec{R})\},$$

where the electric field dependence of the envelope functions is omitted for brevity.

For the given dot size, the hole spin interacts with typically $N \approx 10^4$–10^5 nuclear spins at positions $\vec{R}_i$ ($i = 1, \dots, N$). The full interaction Hamiltonian thus reads (with nuclear spin index i)

$$H_{\text{nuc}} = \sum_i H_I^i$$
$$= \sum_i c_i\{[A(E, \vec{R}_i) + A^\dagger(E, \vec{R}_i)]I_x^i + i[A(E, \vec{R}_i) - A^\dagger(E, \vec{R}_i)]I_y^i + A^z(E, \vec{R}_i)I_z^i\}. \tag{B.2}$$

It can be cast into a pseudo-spin-$\tfrac{1}{2}$ form, where the hole interacts with an effective nuclear magnetic field $\vec{B}_n$, i.e. $H_{\text{nuc}} = \tfrac{\mu_B}{2}\vec{\sigma} \cdot \vec{B}_n$. Contributions proportional to the identity operator of the pseudo-spin-$\tfrac{1}{2}$ space do not change the dynamics and have been omitted. The kth component of $\vec{B}_n$ is calculated by projecting equation (B.2) onto the Pauli matrix σ_k ($k \in \{x, y, z\}$),

$$(\vec{B}_n)_k = \frac{1}{\mu_B}\text{tr}\{\sigma_k H_{\text{nuc}}\} \equiv \frac{1}{\mu_B}\sum_i c_i[g_n^{kx}(E, \vec{R}_i)I_x^i + g_n^{ky}(E, \vec{R}_i)I_y^i + g_n^{kz}(E, \vec{R}_i)I_z^i], \tag{B.3}$$

with

$$g_n^{kx}(E, \vec{R}_i) \equiv 2\text{Re}[\text{tr}\{\sigma_k A(E, \vec{R}_i)\}]$$
$$g_n^{ky}(E, \vec{R}_i) \equiv -2\text{Im}[\text{tr}\{\sigma_k A(E, \vec{R}_i)\}],$$
$$g_n^{kz}(E, \vec{R}_i) \equiv \text{tr}\{\sigma_k A^z(E, \vec{R}_i)\}.$$

IOP Institute of Physics Φ DEUTSCHE PHYSIKALISCHE GESELLSCHAFT

As noted in section 2.1, we employ a quasi-static approximation for the dynamics of the nuclear spins. We further assume that the spins are uncorrelated, e.g. $\langle I_x^i I_x^m \rangle = 0$ for $i \neq m$, and that only a single nuclear spin species with spin I is present. The 'infinite-temperature' density matrix of the nuclear spin ensemble reads $\rho_{\text{nuc}} = \mathbb{1}(2I+1)^{-N}$ [4]. Hence, the mean values $\langle I_x^i \rangle$, $\langle I_y^i \rangle$ and $\langle I_z^i \rangle$ vanish and the variances of the nuclear spin components are $\langle I_x^i I_x^i \rangle = \langle I_y^i I_y^i \rangle = \langle I_z^i I_z^i \rangle = I(I+1)/3$. Furthermore, we can set $c_i = c$. The variances thus read

$$\Delta_k^2 = \langle B_n^k B_n^k \rangle = \left(\frac{c}{\mu_B}\right)^2 \frac{I(I+1)}{3} \sum_i \{[g_n^{kx}(E, \vec{R}_i)]^2 + [g_n^{ky}(E, \vec{R}_i)]^2 + [g_n^{kz}(E, \vec{R}_i)]^2\}. \tag{B.4}$$

The sum in equation (B.4) is performed by a spatial sampling (10^4 points) of the lh and hh envelope functions. The value of the ratio of the variances with respect to Δ_z is $\Delta_x/\Delta_z \approx \Delta_y/\Delta_z \approx 0.12$. We then calculate Δ_x and Δ_y by setting $\Delta_z = 0.1$ mT (this value corresponds to the experimentally determined lower bound of the hole dephasing time, $T_{2,h}^* \approx 100$ ns, see section 2.1). We note that the effective nuclear magnetic field and the variances depend on the externally applied electric field via the electric-field dependence of the envelope functions. The values for Δ_k/Δ_z given here have been calculated for $E = 0$ kV cm^{-1} and $\vec{B} = (0, 0, 10)$ mT.

References

[1] Kroutvar M, Ducommun Y, Heiss D, Bichler M, Schuh D, Abstreiter G and Finley J J 2004 Optically programmable electron spin memory using semiconductor quantum dots *Nature* **432** 81
[2] Amasha S, MacLean K, Radu I P, Zumbühl D M, Kastner M A, Hanson M P and Gossard A C 2008 Electrical control of spin relaxation in a quantum dot *Phys. Rev. Lett.* **100** 046803
[3] Coish W A and Loss D 2005 Singlet–triplet decoherence due to nuclear spins in a double quantum dot *Phys. Rev.* B **72** 125337
[4] Taylor J, Petta J R, Johnson A C, Yacoby A, Marcus C M and Lukin M D 2007 Relaxation, dephasing, and quantum control of electron spins in double quantum dots *Phys. Rev.* B **76** 035315
[5] Petta J R, Johnson A C, Taylor J M, Laird E A, Yacoby A, Lukin M D, Marcus C M, Hanson M P and Gossard A C 2005 Coherent manipulation of coupled electron spins in coherent manipulation of coupled electron spins *Science* **309** 2180
[6] Imamoḡlu A, Knill E, Tian L and Zoller P 2003 Optical pumping of quantum-dot nuclear spins *Phys. Rev. Lett.* **91** 017402
[7] Ramon G and Hu X 2007 Dynamical nuclear spin polarization and the Zamboni effect in gated double quantum dots *Phys. Rev.* B **75** 161301
[8] Reilly D J, Taylor J M, Petta J R, Marcus C M, Hanson M P and Gossard A C 2008 Suppressing spin qubit dephasing by nuclear state preparation *Science* **321** 817
[9] Greilich A, Shabaev A, Yakovlev D R, Efros Al L, Yugova I A, Reuter D, Wieck A D and Bayer M 2007 Nuclei-induced frequency focusing of electron spin coherence *Science* **317** 5846
[10] Eriksson M A, Friesen M, Coppersmith S N, Joynt R, Klein L J, Slinker K, Tahan C, Mooney P M, Chu J O and Koester S J 2004 Spin-based quantum dot quantum computing in silicon *Quantum Inf. Process.* **3** 133
[11] Laurent S, Eble B, Krebs O, Lemaître A, Urbaszek B, Marie X, Amand T and Voisin P 2005 Electrical control of hole spin relaxation in charge tunable InAs/GaAs quantum dots *Phys. Rev. Lett.* **94** 147401
[12] Bulaev D V and Loss D 2005 Spin relaxation and decoherence of holes in quantum dots *Phys. Rev. Lett.* **95** 076805
[13] Gryncharova E I and Perel V I 1977 Relaxation of nuclear spins interacting with holes in semiconductors *Sov. Phys.—Semicond.* **11** 997

IOP **Institute of Physics** Φ DEUTSCHE PHYSIKALISCHE GESELLSCHAFT

[14] Fischer J, Coish W A, Bulaev D V and Loss D 2008 Spin decoherence of a heavy hole coupled to nuclear spins in a quantum dot *Phys. Rev.* B **78** 155329

[15] Testelin C, Bernardot F, Eble B and Chamarro M 2009 Hole spin dephasing time associated with hyperfine interaction in quantum dots *Phys. Rev.* B **79** 195440

[16] Brunner D, Gerardot B D, Dalgarno P A, Wüst G, Karrai K, Stoltz N G, Petroff P M and Warburton R J 2009 A coherent single-hole spin in a semiconductor *Science* **325** 70

[17] Loss D and DiVincenzo D P 1998 Quantum computation with quantum dots *Phys. Rev.* A **57** 120

[18] Kato Y, Myers R C, Driscoll D C, Gossard A C, Levy J and Awschalom D D 2003 Gigahertz electron spin manipulation using voltage-controlled g-tensor modulation *Science* **299** 1201

[19] Doty M F, Scheibner M, Ponomarev I V, Stinaff E A, Bracker A S, Korenev V L, Reinecke T L and Gammon D 2006 Electrically tunable g factors in quantum dot molecular spin states *Phys. Rev. Lett.* **97** 197202

[20] Pingenot J, Pryor C E and Flatté M E 2008 Method for full bloch sphere control of a localized spin via a single electrical gate *Appl. Phys. Lett.* **92** 222502

[21] Andlauer T and Vogl P 2009 Electrically controllable g tensors in quantum dot molecules *Phys. Rev.* B **79** 045307

[22] Andlauer T and Vogl P 2008 Gauge-invariant discretization in multiband envelope function theory and g factors in nanowire dots *Phys. Rev.* B **78** 075317

[23] Andlauer T 2009 Optoelectronic and spin-related properties of semiconductor nanostructures in magnetic fields *Selected Topics of Semiconductor Physics and Technology Vol 105* (Garching: Verein zur Förderung des Walter-Schottky-Inst. der Techn. Univ. München)

[24] Abragam A 1961 *Principles of Nuclear Magnetism* (Oxford: Clarendon)

[25] Merkulov I A, Efros Al L and Rosen M 2002 Electron spin relaxation by nuclei in semiconductor quantum dots *Phys. Rev.* B **65** 205309

[26] Lü C, Cheng J L and Wu M W 2005 Hole spin relaxation in semiconductor quantum dots *Phys. Rev.* B **71** 075308

[27] Lindblad G 1976 On the generators of quantum dynamical semigroups *Commun. Math. Phys.* **48** 119

[28] Heiss D, Schaeck S, Huebl H, Bichler M, Abstreiter G and Finley J J 2007 Observation of extremely slow hole spin relaxation in self-assembled quantum dots *Phys. Rev.* B **76** 241306

[29] Gerardot B D, Brunner D, Dalgarno P A, Öhberg P, Seidl S, Kroner M, Karrai K, Stoltz N G, Petroff P M and Warburton R J 2008 Optical pumping of a single hole spin in a quantum dot *Nature* **451** 441

[30] Trif M, Simon P and Loss D 2009 Relaxation of hole spins in quantum dots via two-phonon processes *Phys. Rev. Lett.* **103** 106601

[31] Havel T F 2003 Robust procedures for converting among Lindblad, Kraus and matrix representations of quantum dynamical semigroups *J. Math. Phys.* **44** 534

[32] O'Brien J L, Pryde G J, Gilchrist A, James D F V, Langford1 N K, Ralph T C and White A G 2004 Quantum process tomography of a controlled-NOT gate *Phys. Rev. Lett.* **93** 080502

[33] Neeley M, Ansmann M, Bialczak R C, Hofheinz M, Katz1 N, Lucero E, O'Connell A, Wang H, Cleland A N and Martinis J M 2008 Process tomography of quantum memory in a Josephson-phase qubit coupled to a two-level state *Nature Phys.* **4** 523

[34] Bialczak R C *et al* 2009 Quantum process tomography of a universal entangling gate implemented with Josephson phase qubits arXiv:0910.1118

[35] Poyatos J F, Cirac J I and Zoller P 1997 Complete characterization of a quantum process: the two-bit quantum gate *Phys. Rev. Lett.* **78** 390

[36] Altepeter J B, Branning D, Jeffrey E, Wei T C, Kwiat P G, Thew R T, O'Brien J L, Nielsen M A and White A G 2003 Ancilla-assisted quantum process tomography *Phys. Rev. Lett.* **90** 193601

[37] Roloff R and Pötz W 2009 Time-optimal performance of Josephson charge qubits: a process tomography approach *Phys. Rev.* B **79** 224516

[38] Schulte-Herbrüggen T, Spörl A, Khaneja N and Glaser S J 2006 Optimal control for generating quantum gates in open dissipative systems arXiv:quant-ph/0609037 v2

[39] Grace M, Brif C, Rabitz H, Walmsley I A, Kosut R L and Lidar D A 2007 Optimal control of quantum gates and suppression of decoherence in a system of interacting two-level particles *J. Phys. B: At. Mol. Opt. Phys.* **40** 103–25

[40] Wenin M and Pötz W 2008 Minimization of environment-induced decoherence in quantum subsystems and application to solid-state-based quantum gates *Phys. Rev.* B **78** 165118

[41] Rebentrost P, Serban I, Schulte-Herbrüggen T and Wilhelm F K 2009 Optimal control of a qubit coupled to a non-Markovian environment *Phys. Rev. Lett.* **102** 090401

[42] Grace M D, Dominy J, Kosut R L, Brif C and Rabitz H 2010 Environment-invariant measure of distance between evolutions of an open quantum system *New J. Phys.* **12** 015001

[43] Storn R and Price K 1997 Differential evolution—a simple and efficient adaptive scheme for global optimization over continuous spaces *J. Global Optim.* **11** 341

[44] Slichter C P 1992 *Principles of Magnetic Resonance* (Berlin: Springer)

[45] Ivchenko E L and Pikus G E 1997 *Superlattices and Other Heterostructures* (Berlin: Springer)

[46] Stoneham A M 2001 *Theory of Defects in Solids* (Oxford: Clarendon)

[47] Sakurai J J 1994 *Modern Quantum Mechanics* (Reading, MA: Addison-Wesley)

[48] Edmonds A R 1996 *Angular Momentum in Quantum Mechanics* (Princeton, NJ: Princeton University Press)

[49] Cornwell J F 1984 *Group Theory in Physics* (New York: Academic)